Supporting Information

Mechanistic insights into the enhanced photocatalytic efficiency of MoS_2-tuned $DyFeO_3$ heterojunction for pollutants degradation

Mohasin Tarek, Ferdous Yasmeen and M. A. Basith*

Nanotechnology Research Laboratory, Department of Physics,

Bangladesh University of Engineering and Technology, Dhaka-1000, Bangladesh.
*Corresponding author(s). E-mail: mabasith@phy.buet.ac.bd

Synthesis of Porous $DyFeO_3$ Nanoparticles

Nanoparticles of $DyFeO_3$ perovskite were synthesized via a sol-gel method as outlined in Figure S1 [1]. Initially, stoichiometric quantities of dysprosium nitrate ($Dy(NO_3)_3 \cdot 5H_2O$) and iron nitrate ($Fe(NO_3)_3 \cdot 9H_2O$) were separately dissolved in 100 ml of deionized water and stirred for 15–20 minutes using a magnetic stirrer to achieve complete dissolution. The two solutions were then combined, and citric acid ($C_6H_8O_7$) was added to act as a chelating agent, stabilizing the metal ions and preventing premature precipitation. Ammonium hydroxide (NH_4OH) was added dropwise to the combined solution to adjust the pH to 7, providing a neutral environment optimal for the subsequent reactions. Ethylene glycol was then introduced into the mixture, serving as both a solvent and a facilitator for forming a polymeric network with the metal cations, essential for creating the gel precursor. The reaction was allowed to proceed at room temperature for four hours, after which the temperature was gradually raised to 200 °C. This temperature increase initiated the combustion process, causing the organic components within the gel to decompose, release gases, and leave behind metal oxide powder. The combustion step was carefully monitored to ensure complete removal of organic residues. The resulting powder was finely ground using an agate mortar to obtain uniform particle size. To enhance the crystallinity and promote the development of a porous structure, the $DyFeO_3$ powder was calcined at 750 °C for 6 hours at a controlled heating rate of 5 °C per minute in a nitrogen atmosphere. The slow and steady heating rate minimized thermal stress, preventing cracking and ensuring structural uniformity. Using nitrogen gas during calcination provided an inert environment, effectively preventing undesired oxidation reactions and managing the release of gases during decomposition. This carefully controlled atmosphere was crucial for achieving the desired porosity and structural properties in the $DyFeO_3$ nanoparticles. Through careful selection of the solvent (deionized water), controlled precursor concentration (ethylene glycol), precise temperature regulation, and optimized nitrogen flow, high-quality, reproducible porous $DyFeO_3$ nanoparticles were obtained.

Synthesis of MoS_2 Nanosheets

MoS_2 nanosheets (NSs) were prepared through an exfoliation technique assisted by ultrasonication [2], starting with bulk MoS_2 powder. First, 500 mg of MoS_2 powder was dispersed in 100 ml of isopropanol. The dispersion was then subjected to ultrasonication in a bath at 50 °C for four hours to facilitate exfoliation. After ultrasonication, the mixture was allowed to settle undisturbed for an additional four hours, enabling the separation of large particles and thicker sheets as a sediment. The clear supernatant, containing exfoliated MoS_2 nanosheets, was carefully collected. This supernatant was subsequently dried in an oven at 120 °C for 12 hours, yielding the final powdered MoS_2 nanosheets.

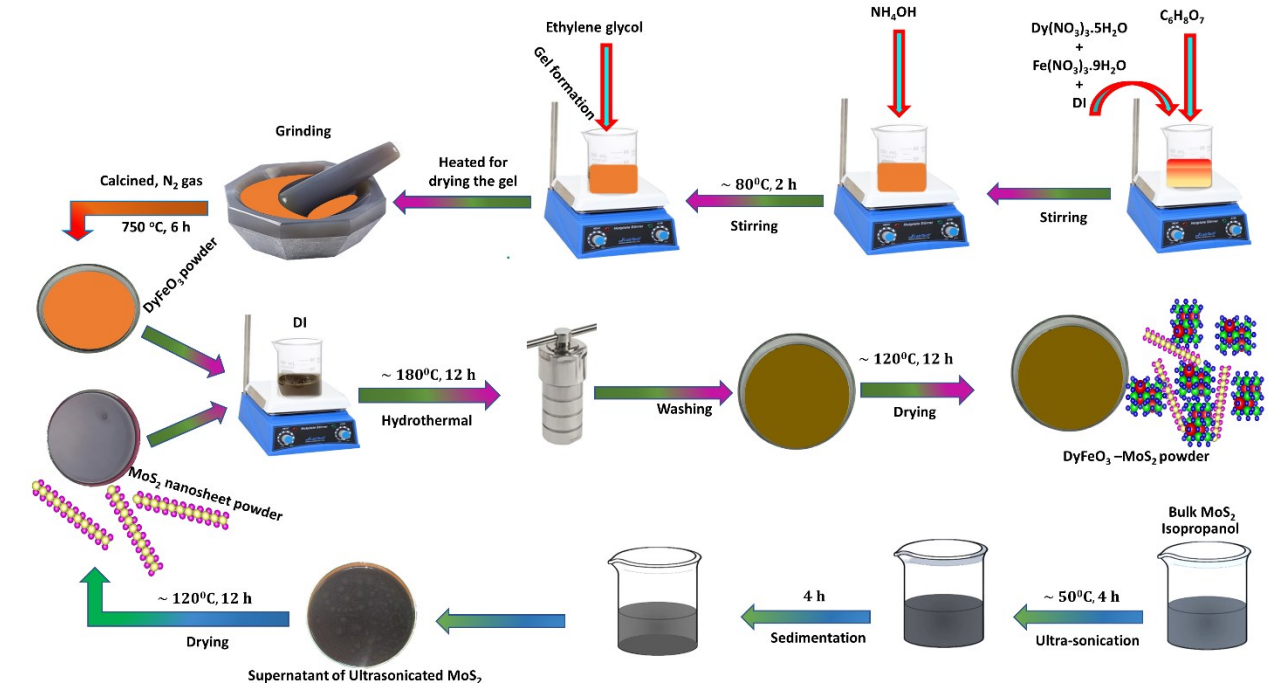

Figure S1. Schematic representation of the synthesis steps of $DyFeO_3$-MoS_2 nanocomposites.

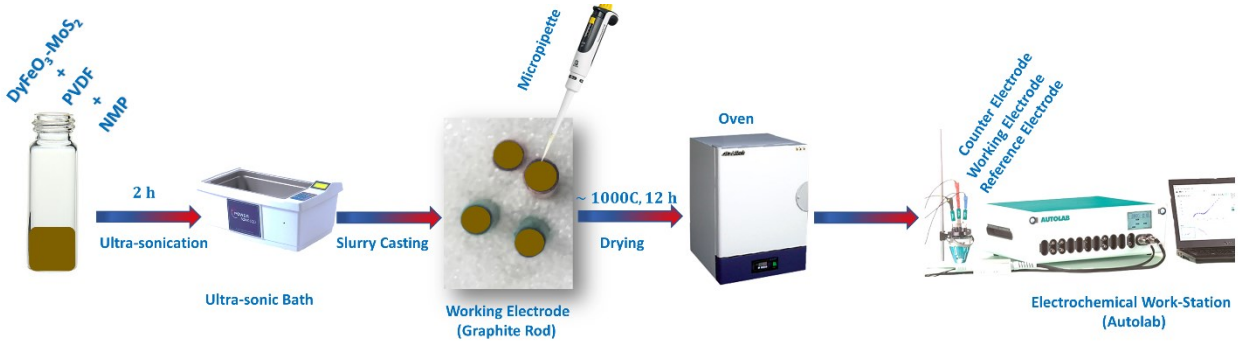

Figure S2. Schematic representation of the preparation of electrode slurry and the experimental setup for electrochemical measurement.

Electrochemical cell setup for Mott-Schottky analysis

A three-electrode system was employed utilizing a 0.5 M Na_2SO_4 aqueous solution as the electrolyte. In this configuration, an Ag/AgCl electrode immersed in a saturated 3.5 M KCl solution served as the reference electrode, while a platinum wire functioned as the counter electrode. To fabricate the working electrode, 20 mg of the synthesized $DyFeO_3$ nanoparticles (constituting 90 wt%) was mixed with 2.22 mg of polyvinylidene fluoride (PVDF; 10 wt%) serving as a binder, and 200 µL of N-methyl-2-pyrrolidone (NMP) as a solvent. This mixture was sonicated for 2 hours to achieve a homogeneous slurry. The resultant slurry was then uniformly cast onto a graphite rod with a surface area of 0.28 cm^2. The coated graphite rod was subsequently dried at 100 °C for 12 hours to ensure complete solvent evaporation and proper adhesion of the active material. This modified graphite rod was subsequently used as the working electrode for Mott-Schottky analysis.

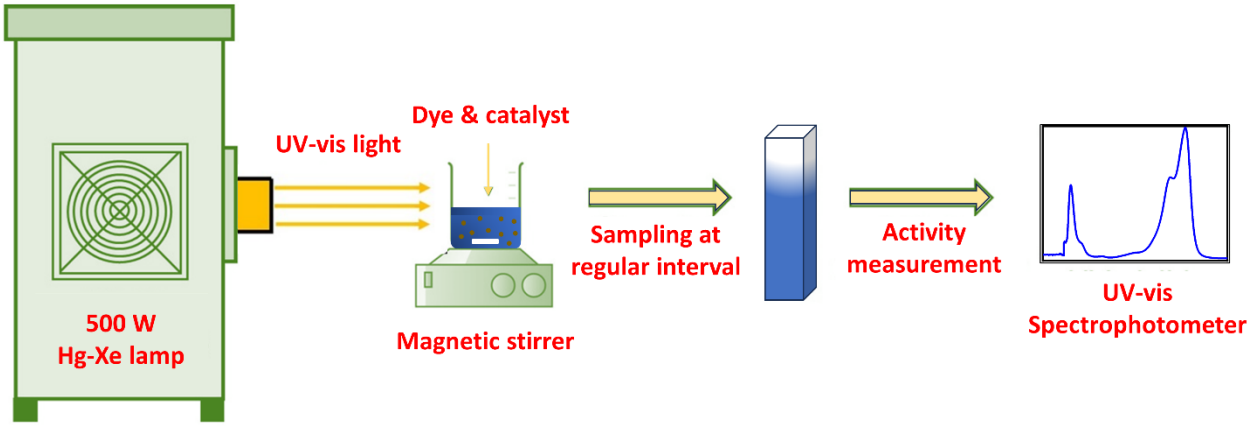

Figure S3. Schematic representation of the experimental setup for photocatalytic degradation of pollutants from waste water.

Experimental setup for photocatalytic degradation of pollutants from water

The schematic representation of the photocatalytic reactor setup for pollutant degradation experiments is illustrated in Fig. S2. The degradation process began with the dissolution of 1.2 mg of Methylene Blue (MB) in 100 mL of distilled water, followed by measuring its absorbance spectrum using a UV-vis spectrophotometer (UV-2600, Shimadzu, Japan). Subsequently, 30 mg of $DyFeO_3$-MoS_2 nanocomposite photocatalyst was added to 50 mL of the MB solution, and the mixture was stirred in the dark for one hour to establish adsorption-desorption equilibrium between the photocatalyst and MB. The photocatalytic reaction was then initiated by illuminating the

solution with a 500 W Hg-Xn lamp, providing an irradiance of 100 mW cm^{-2} in the solar spectrum. After 30 minutes of irradiation, 6 mL of the suspension was withdrawn and centrifuged at 6500 rpm for 2 minutes. The absorbance spectrum of the supernatant was measured to determine the remaining MB concentration

For the degradation of Levofloxacin (LFX), a solution was prepared by dissolving 1 mg of LFX in 100 mL of distilled water. Then, 15 mg of $DyFeO_3$-MoS_2 nanocomposite photocatalyst was added to 50 mL of the LFX solution, and the same procedures as those used for MB degradation were followed.

Active species trapping experiments were performed under solar illumination, utilizing four different scavengers: isopropanol (IPA) for hydroxyl radicals (•OH), acrylamide for superoxide radicals ($\bullet O^{2-}$), potassium dichromate ($K_2Cr_2O_7$) for electrons (e^-), and EDTA-2Na for holes (h^+). The degradation efficiency was evaluated by adding 1.5 mM of each scavenger to the reaction mixture.

In the activation energy determination experiment, a solution of 1 mg LFX in 100 mL distilled water was prepared, and 30 mg of $DyFeO_3$-MoS_2 nanocomposites were added to 50 mL of this solution. After stirring in the dark for one hour to reach adsorption-desorption equilibrium, the solution was exposed to a solar simulator. The absorbance spectrum was measured after 30 minutes of illumination at various temperatures. This experiment was also repeated without the addition of $DyFeO_3$-MoS_2 nanocomposites to the LFX solution for comparison.

Crystallite size calculation of $DyFeO_3$-MoS_2 nanocomposites:

The crystallite size was determined using the Scherrer equation [1], which correlates the broadening of XRD peaks with the size of the crystalline domains. The equation is expressed as:

$$D = \frac{k\lambda}{\beta \cos\theta}$$

Here, D represents the crystallite size, K is the shape factor (commonly taken as 0.9), λ denotes the wavelength of the X-ray radiation, β is the full width at half maximum (FWHM) of the diffraction peak, and θ is the Bragg angle.

Table S1 Crystallographic parameters of various concentrations of MoS_2 nanosheets incorporated $DyFeO_3$-MoS_2 nanocomposites from Rietveld refinement XRD spectra. measurement.

Sample	Constituent	Crystallographic phase	Space group	a (Å)	b (Å)	c (Å)	d-spacing (Å)	Crystallite size (nm)	χ^2
$DyFeO_3$-MoS_2 (90:10)	$DyFeO_3$	Orthorhombic	*Pnma*	5.59234	7.61341	5.29576	2.704	36.10	2.35
	MoS_2	Hexagonal	*P 63/m m c*	3.14185	3.14185	12.34043	6.184		
$DyFeO_3$-MoS_2 (80:20)	$DyFeO_3$	Orthorhombic	*Pnma*	5.31011	5.59755	7.62586	2.709	37.49	2.15
	MoS_2	Hexagonal	*P 63/m m c*	3.14592	3.14592	12.35494	6.383		
$DyFeO_3$-MoS_2 (70:30)	$DyFeO_3$	Orthorhombic	*Pnma*	5.58638	7.61327	5.29293	2.705	35.51	2.31
	MoS_2	Hexagonal	*P 63/m m c*	3.15607	3.15607	12.28868	6.257		

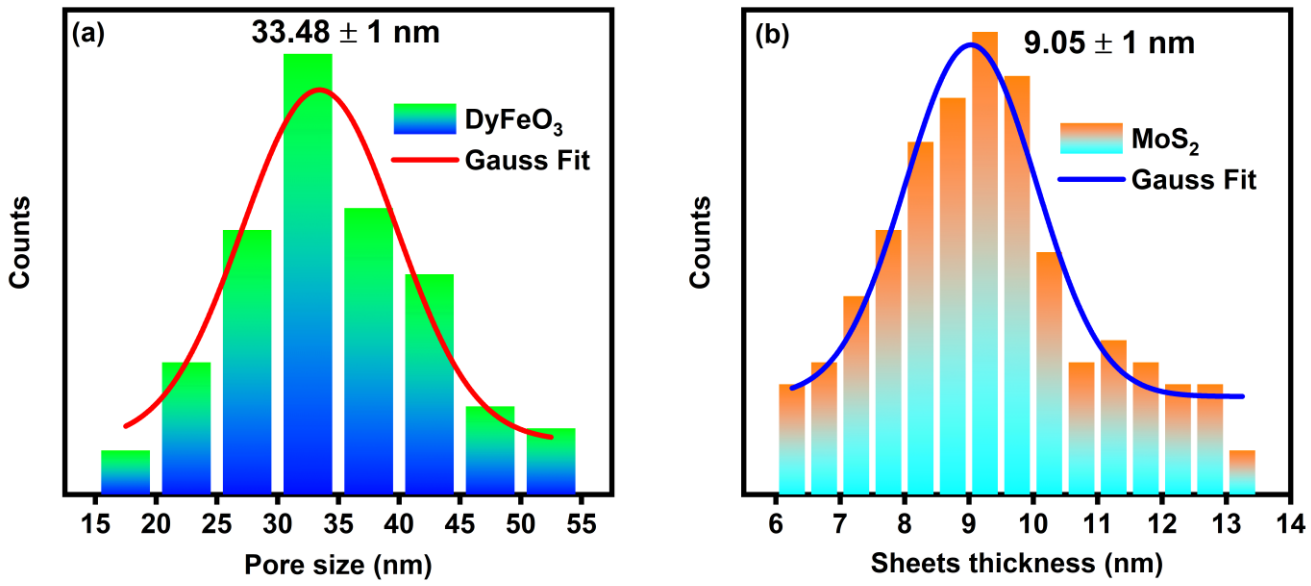

Figure S4. (a) Pore size distribution histogram of porous $DyFeO_3$ nanoparticles and (b) sheet thickness distribution histogram of MoS_2 nanosheets from FESEM image of $DyFeO_3$-MoS_2 (80:20) nanocomposite.

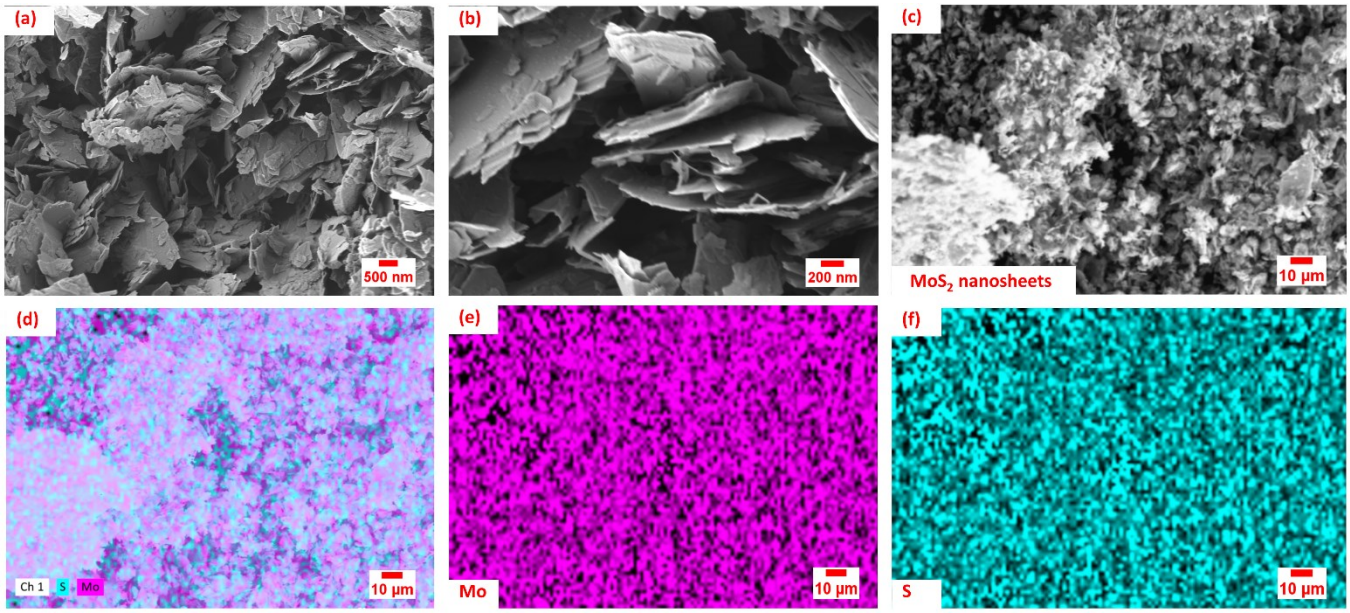

Figure S5. (a) Low and (b) high magnification FESEM images of MoS_2 nanosheets. (c-d) FESEM image of the as-prepared MoS_2 nanosheets to demonstrate the distribution of (e) Mo and (f) S atoms throughout the nanocrystal.

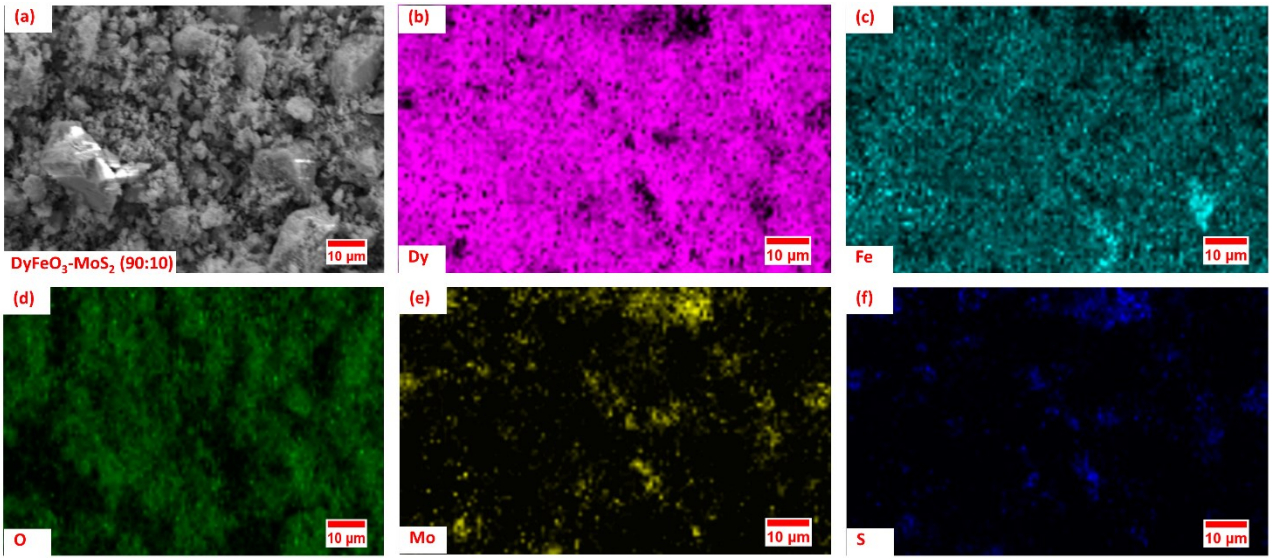

Figure S6. (a) FESEM image of the as-prepared $DyFeO_3$-MoS_2 (90:10) nanocomposite to demonstrate the distribution of (b) Mo (c) Fe, (d) O, (e) Mo and (f) S atoms throughout the nanocomposite.

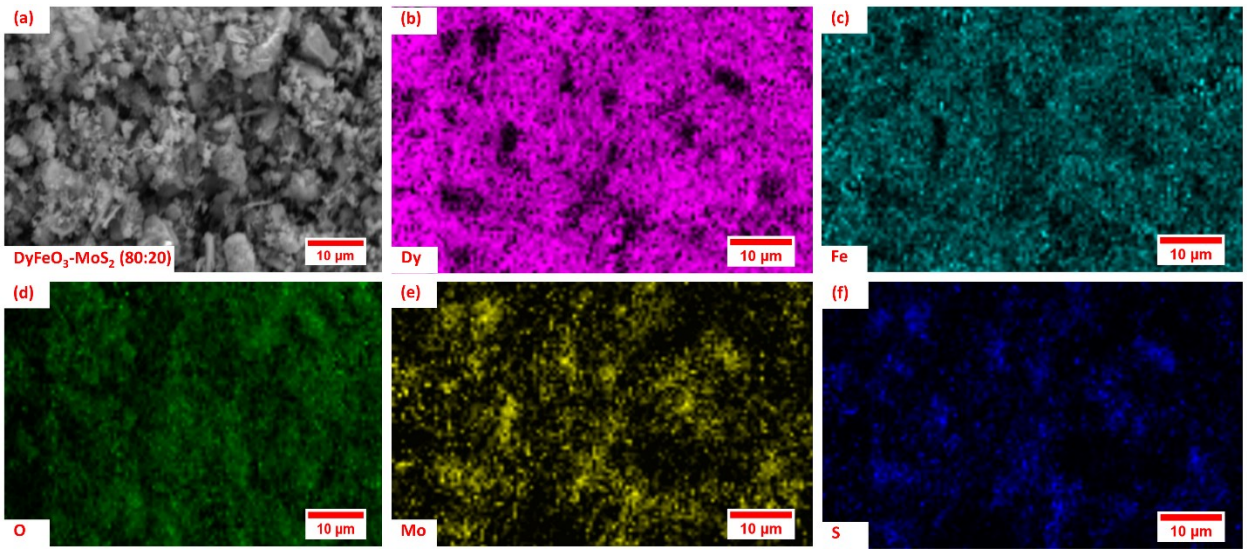

Figure S7. (a) FESEM image of the as-prepared $DyFeO_3$-MoS_2 (80:20) nanocomposite to demonstrate the distribution of (b) Mo (c) Fe, (d) O, (e) Mo and (f) S atoms throughout the nanocomposite.

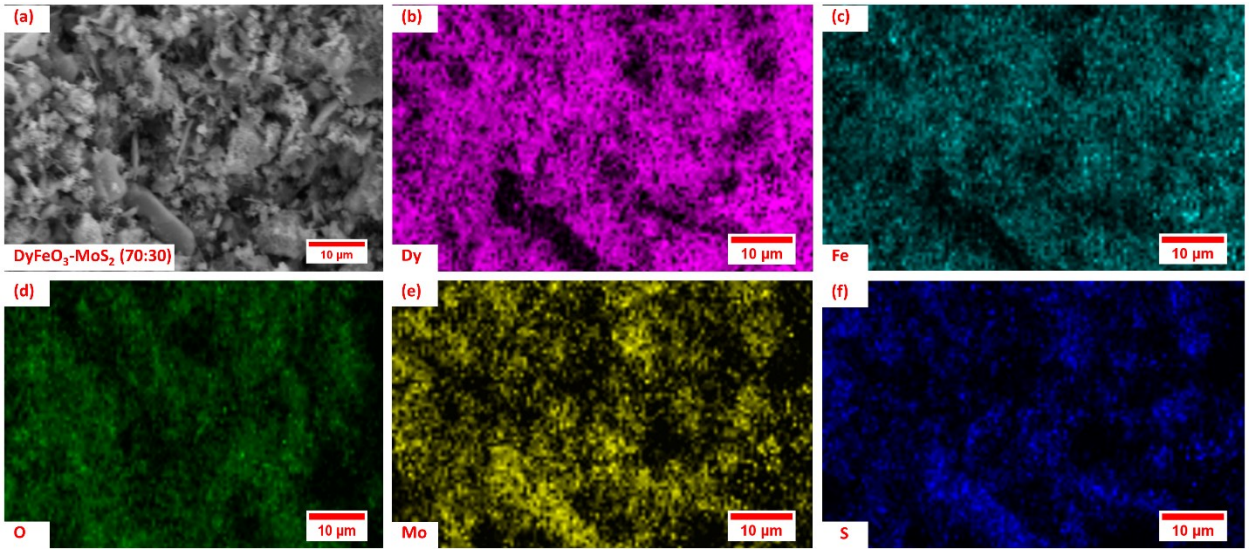

Figure S8. (a) FESEM image of the as-prepared $DyFeO_3$-MoS_2 (70:30) nanocomposite to demonstrate the distribution of (b) Mo (c) Fe, (d) O, (e) Mo and (f) S atoms throughout the nanocomposite.

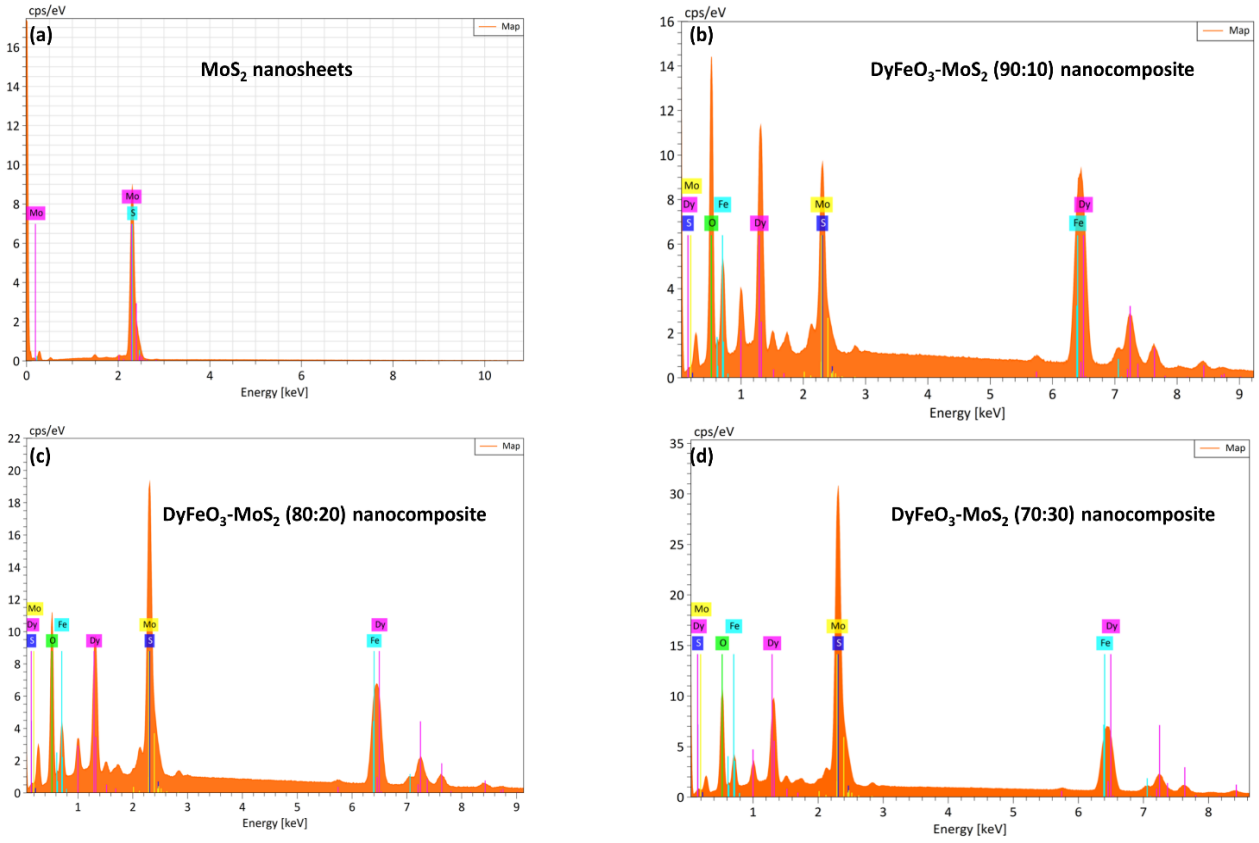

Figure S9. Energy Dispersive X-ray (EDX) spectra of (a) MoS_2 nanosheets, (b) $DyFeO_3$-MoS_2 (90:10), (c) $DyFeO_3$-MoS_2 (80:20) and (d) $DyFeO_3$-MoS_2 (70:30) nanocomposites.

Table S2. Mass and Atom percentages of elements in MoS_2 nanosheets, and various concentrations of MoS_2 incorporated $DyFeO_3$-MoS_2 nanocomposites as obtained via EDX and theoretical analysis.

Sample	Element	Mass (%) (theoretical)	Mass (%) (experimental)	Atom (%) (theoretical)	Atom (%) (experimental)
MoS_2	Mo	59.94	60.49	33.33	33.50
	S	40.06	39.51	66.67	66.50
$DyFeO_3$-MoS_2 (90:10)	Dy	54.91	55.31	18	19.04
	Fe	18.87	17.08	18	18.76
	O	16.22	18.04	54	52.20
	Mo	5.99	6.02	3.33	4.12
	S	4.01	3.55	6.67	5.88
$DyFeO_3$-MoS_2 (80:20)	Dy	48.81	50.02	16	16.90
	Fe	16.78	16.10	16	15.87
	O	14.42	14.70	48	47.50
	Mo	11.99	12.11	6.67	7.10
	S	8.01	7.07	13.33	12.63
$DyFeO_3$-MoS_2 (70:30)	Dy	42.71	40.30	14	13.20
	Fe	14.68	15.70	14	14.50
	O	12.61	13.20	42	41.85
	Mo	17.98	18.40	9.99	10.30
	S	12.02	12.40	20.01	20.15

Table S3. The XPS spectrum of $DyFeO_3$-MoS_2 (80:20) nanocomposite revealed several distinct peaks corresponding to the oxidation states of Dy, Fe, O, Mo, and S.

Element	Orbital	Peaks	Binding energy (eV)
Dy	Dy 3d	$3d_{3/2}$ (Dy^{3+})	1335.41
		$3d_{5/2}$ (Dy^{3+})	1297.40
Fe	Fe 2p	satellite	733.54
		$2p_{1/2}$ (Fe^{3+})	726.13
		$2p_{1/2}$ (Fe^{2+})	724.41
		satellite	719.43
		$2p_{3/2}$ (Fe^{3+})	712.36
		$2p_{3/2}$ (Fe^{2+})	710.88
O	O 1s	O_{OH}^-	532.95
		$O_{vcan.}$	531.33
		O^{2-} (metal oxide)	529.96
Mo	Mo 3d	$3d_{3/2}$ (Mo^{6+})	236.69
		$3d_{5/2}$ (Mo^{4+})	232.48
		$3d_{3/2}$ (Mo^{4+})	229.28
		Mo-S S 2s	226.36
S	S 2p	satellite	169.61
		$2p_{1/2}$	163.57
		$2p_{3/2}$	162.36

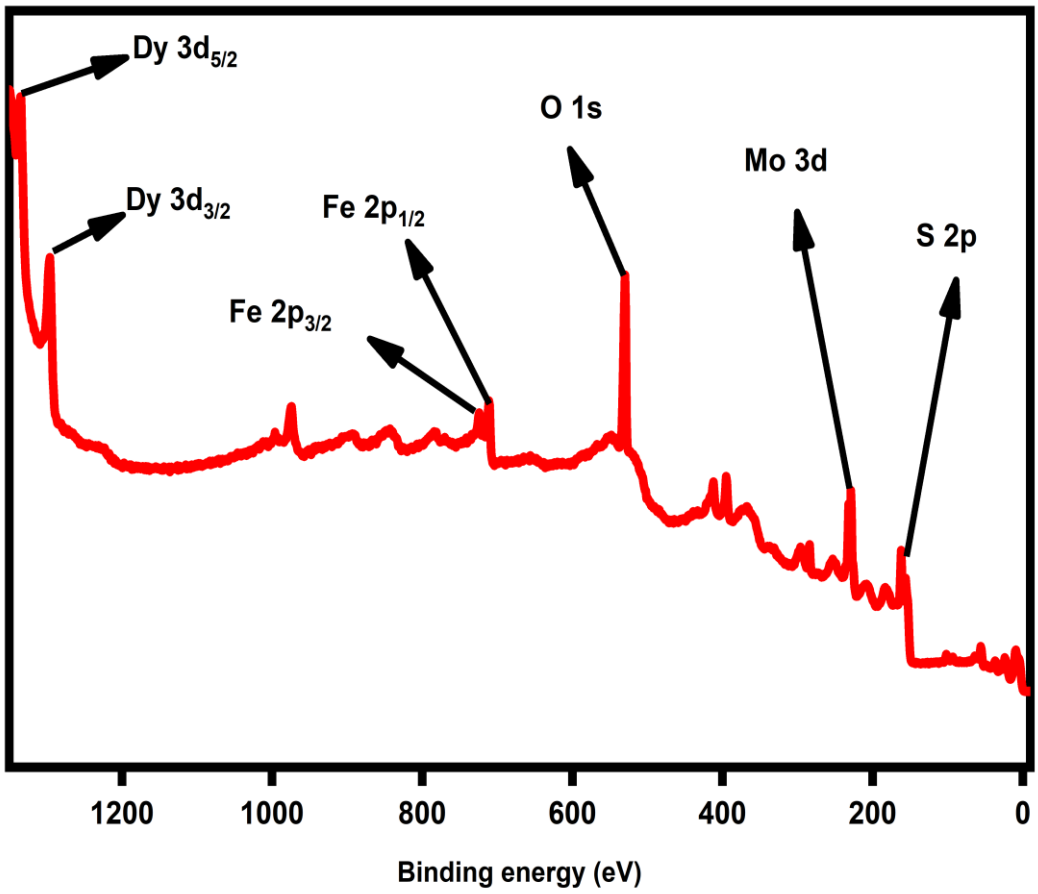

Figure S10 The XPS full survey spectrum of $DyFeO_3$-MoS_2 (80:20) nanocomposite revealed several distinct peaks corresponding to the oxidation states of Dy, Fe, O, Mo, and S.

Band-edge position calculation:

The band edge positions were experimentally determined using Mott-Schottky analysis [1,3]. For an n-type semiconductor, the negative x-intercept value, corresponding to the flat band potential (E_{fb}) with respect to the Ag/AgCl electrode, was converted into the conduction band minimum (E_{CBM}) relative to the NHE electrode using the following equation:

$$E_{CBM} = E_{fb\ (vs.\ Ag/AgCl)} + 0.197 - 0.1\ (V\ vs.NHE)$$

For a p-type semiconductor, the positive x-intercept value, also corresponding to E_{fb} with respect to the Ag/AgCl electrode, was converted into the valence band maximum (E_{VBM}) relative to the NHE electrode using the equation:

$$E_{VBM} = E_{fb\ (vs.\ Ag/AgCl)} + 0.197 + 0.1\ (V\ vs.NHE)$$

Subsequently, the value of E_{VBM} for the n-type semiconductor and E_{CBM} for the p-type semiconductor was determined using the following relation:

$$E_g = E_{VBM} - E_{CBM}$$

where E_g represents the optical bandgap, which was obtained from Tauc plots.

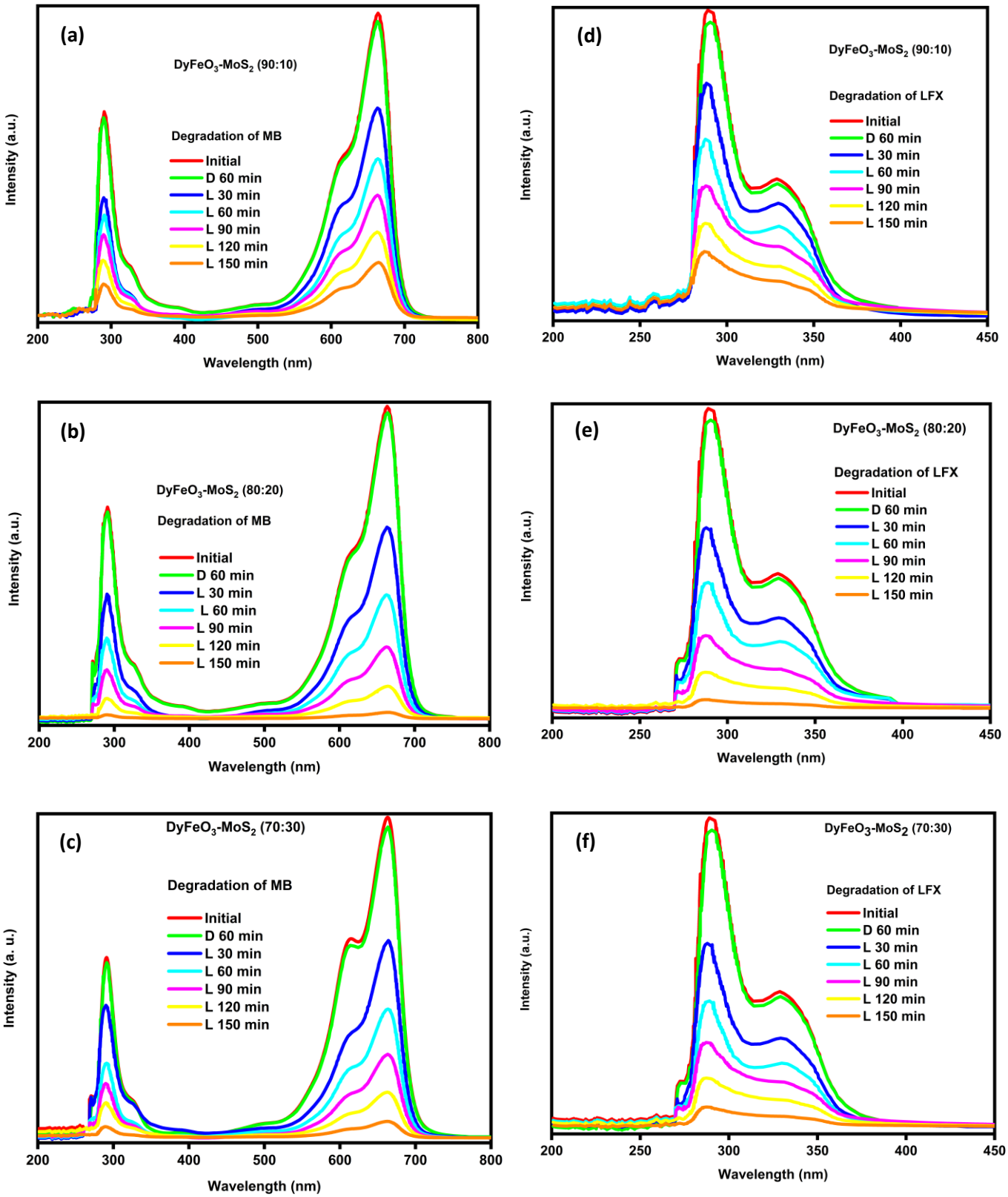

Figure S11. (a-c) UV-vis absorbance spectra of the degradation of methylene blue (MB) with the presence of (a) $DyFeO_3$-MoS_2 (90:10), (b) $DyFeO_3$-MoS_2 (80:20), and (c) $DyFeO_3$-MoS_2 (70:30) nanocomposites. (d-f) UV-vis absorbance spectra of the degradation of methylene blue (MB) with the presence of (d) $DyFeO_3$-MoS_2 (90:10), (e) $DyFeO_3$-MoS_2 (80:20), and (f) $DyFeO_3$-MoS_2 (70:30) nanocomposites.

Apparent Quantum Yield (AQY) calculation

Step 1: Degraded pollutant molecule calculation

Detail	Unit	MB ($DyFeO_3$-MoS_2 (90:10))	MB ($DyFeO_3$-MoS_2 (80:20))	MB (DyFeO3-MoS2 (70:30))	LFX ($DyFeO_3$-MoS_2 (90:10))	LFX ($DyFeO_3$-MoS_2 (80:20))	LFX ($DyFeO_3$-MoS_2 (70:30))
Pollutant solution	L	0.05	0.05	0.05	0.05	0.05	0.05
Pollutant concentration	g/L	0.012	0.012	0.012	0.01	0.01	0.01
Pollutant weight in solution	g	0.0006	0.0006	0.0006	0.0005	0.0005	0.0005
Molecular weight	g/mol	319.85	319.85	319.85	361.368	361.368	361.368
No. of moles in a solution	mol	1.88×10^{-6}	1.88×10^{-6}	1.88×10^{-6}	1.38×10^{-6}	1.38×10^{-6}	1.38×10^{-6}
No. of molecules in a mole	molecules/mol	6.02×10^{23}	6.02×10^{23}	6.02×10^{23}	6.02×10^{23}	6.02×10^{23}	6.02×10^{23}
Total no. of pollutant molecules	molecules	1.13×10^{18}	1.13×10^{18}	1.13×10^{18}	8.31×10^{17}	8.31×10^{17}	8.31×10^{17}
Degradation percentage	%	82	98	92	79	97	92
No. of degraded molecules	molecules	9.27×10^{17}	1.11×10^{18}	1.04×10^{18}	6.56×10^{17}	8.06×10^{17}	7.65×10^{17}

Step 2: Photon energy calculation

Wavelength of light $\lambda = 440$ nm $= 440 \times 10^{-9}$ m

Energy of one photon $E = \frac{hc}{\lambda} = \frac{6.6\times10^{-34}\times3\times10^{8}}{440\times10-9} = 4.50 \times 10^{-19}\ Joules$

The total energy of light falling per second per unit area is

$$E_{Total} = 100\ mW\ cm^{-2} = 100 \times 10^{-3} \times 10^{4} W\ m^{-2} = 1000\ W\ m^{-2}$$

Number of Photon $= \frac{E_{Total}}{\mathrm{E}} = \frac{1000}{4.50\times10^{-19}} = 2.22 \times 10^{21}$

Area of exposed solution =

$$\frac{2\pi rl}{2} = \pi rl$$

Total number of Photon falling on the solution (Number of incident Photon) = Number of Photon × Area of exposed solution

Apparent Quantum Yield (AQY) = $\frac{Number\ of\ degraded\ molecule}{Number\ of\ incident\ photon} \times 100$

Irradiation time (min.)	Area of exposed solution (m^2)	Number of incident photon	Apparent Quantum Yield (%) in MB ($DyFeO_3$-MoS_2 (90:10))	Apparent Quantum Yield (%) in MB ($DyFeO_3$-MoS_2 (80:20))	Apparent Quantum Yield (%) in MB ($DyFeO_3$-MoS_2 (70:30))	Apparent Quantum Yield (%) in LFX ($DyFeO_3$-MoS_2 (90:10))	Apparent Quantum Yield (%) in LFX ($DyFeO_3$-MoS_2 (80:20))	Apparent Quantum Yield (%) in LFX ($DyFeO_3$-MoS_2 (70:30))
150	0.001411	3.13×10^{18}	29.62	35.46	33.23	20.96	25.75	24.44

References:

[1] M. Tarek, F. Yasmeen and M. A. Basith, *J. Mater. Chem. A*, 2024, **12**, 25475–25490.
[2] M. Tarek and M. A. Basith, *J. Mater. Chem. C*, 2023, **11**, 16605–16622.
[3] M. A. Adib, F. Sharmin and M. A. Basith, *Nanoscale Adv.*, 2023, **5**, 6194–6209.